IEEE Access
Multidisciplinary | Rapid Review | Open Access Journal

Received May 5, 2019, accepted May 23, 2019, date of publication June 4, 2019, date of current version June 20, 2019.

Digital Object Identifier 10.1109/ACCESS.2019.2920736

Multi-UAV Rapid-Assessment Task-Assignment Problem in a Post-Earthquake Scenario

MONING ZHU[1,3], XIAOXIA DU[2], XUEHUA ZHANG[2], HE LUO[1,3], AND GUOQIANG WANG[1,3]

[1]School of Management, Hefei University of Technology, Hefei 230009, China
[2]National Earthquake Response Support Service, Beijing 100049, China
[3]Key Laboratory of Process Optimization and Intelligent Decision-Making, Ministry of Education, Hefei 230009, China

Corresponding author: He Luo (luohe@hfut.edu.cn)

This work was supported in part by the National Natural Science Foundation of China under Grant 71871079, Grant 71671059, and Grant 71401048, in part by the National Key Research and Development Program of China under Grant 2017YFB0504104, in part by the Anhui Provincial Natural Science Foundation under Grant 1808085MG213 and Grant 1508085MG140, and in part by the Fundamental Research Funds for the Central Universities under Grant JZ2018HGBZ0128.

ABSTRACT The rapid assessment of earthquake-stricken regions immediately after a seismic event is crucial for earthquake relief operations. Since unmanned aerial vehicles (UAVs) can quickly reach the affected areas and obtain images, they are widely used in the post-earthquake rapid assessment. However, sensor noise and other unavoidable errors can affect the quality of images acquired by sensors attached to the UAVs, which can, in turn, reduce the quality of the assessment. We defined a new problem in the application of multiple UAVs in the rapid assessment of earthquake-stricken regions. The rapid-assessment task-assignment problem (RATAP) was used to construct the assignment plan for multiple UAVs in a rapid-assessment task while considering the weights of potential targets, the endurance of the UAVs, and the sensor errors. The RATAP was formulated as a variant of the team orienteering problem (TOP) called the revisit-allowed TOP with reward probability (RTOP-RP). We then developed an efficient hybrid particle swarm optimization with simulated annealing (HPSO-SA) algorithm, which produced a high-quality solution for the RATAP, and confirmed the effectiveness and rapidity of our algorithm through numerical experiments. Finally, we conducted a case study based on real-world data from the 2008 Wenchuan earthquake in China to demonstrate our approach.

INDEX TERMS Post-earthquake, multiple unmanned aerial vehicles, rapid-assessment task-assignment problem, target-revisit-allowed strategy.

I. INTRODUCTION

In the last decade, the number of earthquakes and the size of affected populations have grown, according to the biennial *Global Disaster Risk Assessment Report* [1]–[5] released by the United Nations International Strategy for Disaster Reduction (UNISDR). In 2017, earthquakes caused the loss of hundreds of billions of dollars and affected several million people globally [6]. The rapid assessment of earthquake-stricken regions immediately after a seismic event is crucial for earthquake relief operations, especially in remote regions where the existing communication system may be poor [7]. The rapid assessment operation may start as soon as possible after the earthquake, and is typically completed within 72 hours. Some of the main purposes of rapid assessment are to assess the damage of the population gathering points (such as schools and hospitals) and to understand the basic needs of disaster victims, including water, food, non-food items, and shelter. The results of rapid assessment have been shown to directly affect the allocation of disaster relief resources and search-and-rescue operations [8], [9]. High-quality rapid-assessment results have been found to ensure efficient allocation of resources, ultimately minimizing damage and casualties [10], [11]. In the last decade, because of their speed, flexibility, and efficiency, unmanned aerial vehicles (UAVs) have been routinely used by many rescue agencies for rapid assessment after disasters [12]–[14]. UAV-assisted architecture affords flexible deployment and low operational costs, especially when traditional communication systems have been damaged by natural disasters [15]. In the 2008 Wenchuan M8.0 earthquake in China [16], [17], the 2009 L'Aquila M7.2 earthquake in

The associate editor coordinating the review of this manuscript and approving it for publication was Kuo-Ching Ying.

Italy [18], [19], the 2010 M7.0 earthquake in Haiti [20], the 2011 M9.0 earthquake and tsunami in East Japan [21], the 2013 Lushan M7.0 earthquake in China [22], the 2014 Iquique M8.2 earthquake in Chile [23], and the 2016 Kumamoto M7.3 earthquake in Japan [24], UAVs were used to collect many images of earthquake-stricken regions through the remote control of professional operators immediately after the disaster. Based on these images, the damage to buildings in earthquake-stricken areas was mapped and assessed, which provided useful information for rescue operations.

When performing a rapid assessment after an earthquake, UAVs have been shown to quickly reach the disaster area and capture images and videos of multiple potential targets in a short period of time [25], where potential targets are the task point targets provided by experts from a relief agency and based on integrated characteristics and available information of the targets [26]. For the rapid assessment of multiple point targets, the paths of multiple UAVs must be coordinated and optimized to maximize the utility of the UAVs and improve the quality of their rapid assessment. Operations research (OR) has been found to help UAVs improve the efficiency and efficacy of humanitarian aid [27]. Otto *et al.* [28] reviewed the literature on civil aircraft optimization methods for UAVs. Similarly, Trigui *et al.* [29] applied a traveling salesman problem (TSP) variant model to solve the multi-UAV emergency-response problem for multiple potential targets. Multiple objectives, including total trips, maximum trips, and mission time, can be optimized using the model. The vehicle routing problem (VRP) model [30] was used to construct the shortest assessment routes for a fleet of UAVs to visit all point targets in an affected area without considering the UAVs' transport capacity. Moreover, Huang *et al.* [31] used a VRP variant model to solve the path-optimization problem for the rapid distribution of relief materials. A team orienteering problem (TOP) variant model proposed by Balcik [32] was used to construct an assessment plan to cover different point targets in a balanced way. Site selection and routing decisions of post-disaster rapid assessment can be solved using the objective function, which maximizes the minimum coverage ratio of different characteristic point targets with duration constraints. Some OR models were also applied to solve the routing-optimization problem in the rapid-assessment stage, such as the continuous approximation method [33], which minimized the total visit time for vehicles accessing all targets, and the mixed integer programming method [34], which optimized the time interval between consecutive visits to the same target.

Analysis of the above literature indicated that when the number of potential targets was small, or the targets were relatively concentrated and the UAVs could cover all the targets, OR models, such as the TSP and VRP, could determine the task assignment and path planning of the UAVs. The TOP, which can solve the problem of target selection, was more efficient when the number of potential targets was large, or when they were widely distributed. A UAV, however, cannot access all the potential targets in a certain period of time. Access to important potential targets can improve the reward of rapid assessment in a post-earthquake scenario. The importance of potential targets is generally based on their characteristics, which include the distance from the epicenter, the type of building, and the population size. Before the assessment is performed by a UAV, experts from relief agencies must determine the importance of every potential target, which is described in the form of a weight. In an actual post-earthquake scenario, because the number of UAVs that can perform assessment tasks will be limited, and each UAV will be constrained by its endurance capability, we believe that the TOP model is more suitable for rapid assessment, as it can optimize the UAV task-assignment problem.

Furthermore, in the implementation of post-disaster rapid assessment, sensor noise and other unavoidable errors [35] can affect the credibility of the information collected by a UAV, which in turn can reduce the effectiveness of the rapid assessment. Thus, we proposed a target-revisit-allowed strategy, and the expected reward was used to evaluate the effectiveness of a rapid-assessment task. The expected reward of a UAV rapid-assessment task was maximized by selecting appropriate potential targets and optimizing the visit order and the number of visits of multiple UAVs to these targets. The main contributions of this study were as follows:

(1) We introduced and defined the rapid-assessment task-assignment problem (RATAP). The problem was as follows. We maximized the expected reward of the rapid-assessment task-scheme by selecting appropriate potential targets to be accessed by UAV fleets and then determining the order of access and the number of visits to each potential target under the constraints of their endurance capability and the detection error of sensors carried by the UAVs. The RATAP was a practical problem that is faced in the emergency rescue process in a post-earthquake scenario. In this study, the RATAP was modeled as a revisit-allowed TOP with reward probability (RTOP-RP). The model's objective function maximized the expected reward, as represented by the effective information of a potential target of the rapid-assessment task. The expected reward was calculated by multiplying the weight of a potential target by the probability of a successful collection of valid information about that target.

(2) A new task-assignment strategy called the target-revisit-allowed strategy was proposed, which considered the impact of sensor errors on rapid-assessment tasks. We also suggested a quantitative analysis model to evaluate the effectiveness of a rapid-assessment task-assignment scheme. When compared with the revisit-forbidden strategy, the revisit-allowed strategy was found to improve the effectiveness of a rapid-assessment task-scheme.

(3) The hybrid particle swarm optimization with simulated annealing (HPSO-SA) algorithm was specifically designed for the RATAP. According to the actual needs of the rapid-assessment task, the algorithm for solving the RTOP-RP model mainly emphasized rapidity and robustness. Therefore, we innovatively combined the classical particle swarm

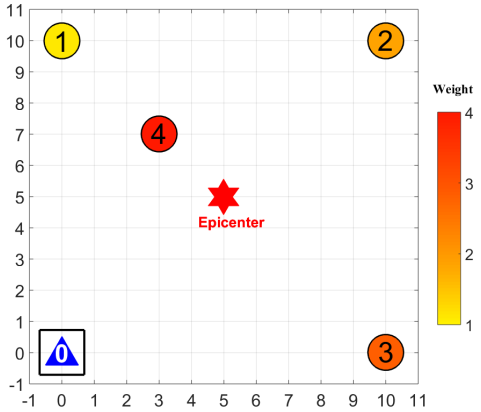

FIGURE 1. Scenario where a rapid assessment after an earthquake is required.

optimization (PSO) and simulated annealing (SA) algorithms by designing an algorithm framework, solution encoding method, particle updating operation, and disturbance operation to form the HPSO-SA algorithm which was specifically designed for solving the RTOP-RP model. The performance of the algorithm was demonstrated through numerical experiments. Finally, we illustrated how to use our approach in the real world with a case study based on data from the 2008 Wenchuan earthquake in China. The results showed that HPSO-SA algorithm could obtain a high-quality, feasible RATAP solution in a short period of time, which represented a multi-UAV task-assignment scheme for rapid assessment.

The rest of this paper is organized as follows: In Section II, an illustrative example of small instances in which it was possible to obtain optimal solutions was conducted to develop insights into the RATAP's characteristics. In Section III, the multi-UAV rapid-assessment task-assignment problem is defined, and its mathematical model is given. The HPSO-SA algorithm is discussed in Section IV, and the computational results of the numerical experiments are presented in Section V. A case study and the analysis of the Wenchuan earthquake is presented in Section VI. The summary work and the future scope of the work are discussed in Section VII.

II. ILLUSTRATIVE EXAMPLE OF RATAP

In this section, we analyze the characteristics of the RATAP through an illustrative example. Fig. 1 depicts a scenario when a rapid assessment after an earthquake was required. The epicenter was located in the center of the earthquake-stricken region, which included four earthquake-stricken points. The weights of the points were determined by the relief experts based on their characteristics, which included the distance from the epicenter and the population. The relief organization dispatched two UAVs to access the four potential targets. The UAVs departed from point zero, completed the rapid-assessment task, and returned to point zero. The endurance capacity of each UAV was 30 units, and the detection-error probability of a UAV-carried sensor was 20%.

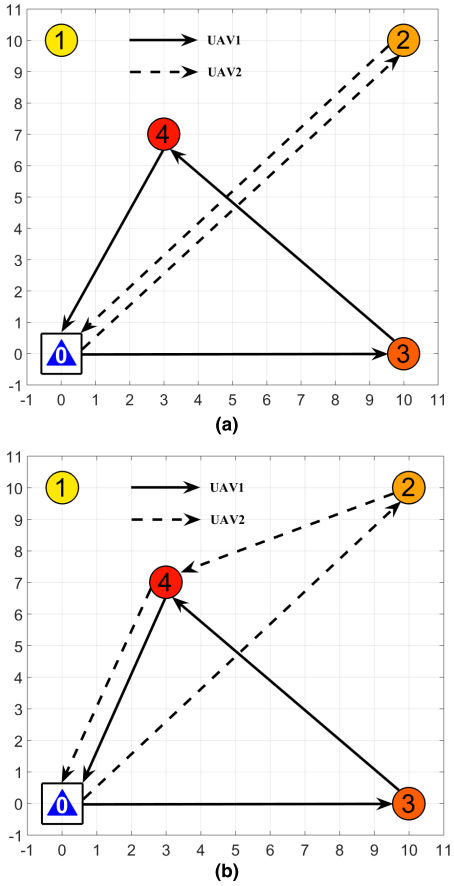

FIGURE 2. Multi-UAV rapid-assessment task-allocation scheme after an earthquake. (a)Task-allocation scheme 1; (b)Task-allocation scheme 2.

When the above problem was modeled as a TOP with UAV endurance, the two UAVs could not access all four potential targets, and each one was only visited once. In all the possible task-allocation schemes, the two UAVs could only visit three of the four potential targets. By considering the weights of the potential targets, we obtained a task-allocation scheme that maximized the sum of weights, as shown in Fig. 2(a). In the scheme, UAV1 started at #0, sequentially visited targets 3 and 4, and returned to #0, with a flight distance of 27.52; UAV2 started at #0, visited target 2, and returned to #0, for a flight distance of 28.28. The total reward of the task-assignment scheme was 9. If the detection-error probability of the sensor carried by a UAV was considered, then the expected reward of the task-allocation scheme was 7.2. The calculation method for the expected reward is described in Section III.

When the above problem was modeled as a RATAP, each potential target could be accessed multiple times. For example, target 4 could be accessed twice, and the task- allocation scheme, as shown in Fig. 2(b), was obtained. In this scheme, UAV1 started at #0, sequentially accessed targets 3 and 4, and returned to #0, for a flight distance of 27.52. UAV2 started at #0, accessed targets 2 and 4, and returned to #0, with a total flight distance of 29.37. The weights of the task-assignment scheme still added up to 9, but the expected reward was 7.84.

TABLE 1. Definitions of sets, indices, parameters, and variables.

Notation	Explanation
$\mathbf{U}$	set of UAVs, $\mathbf{U}=\{1, 2,\ldots, k,\ldots, K\}$.
$\mathbf{T}$	set of potential targets, $\mathbf{T}=\{1, 2,\ldots, i,\ldots, L\}$.
k	index of UAVs, $k \in \mathbf{U}$.
h, i, j	index of potential targets, $h,i,j \in \mathbf{T}$.
0, L+1	indices representing a UAV's start and end points, respectively.
$\mathbf{A}$	set of all points, $\mathbf{A}=\{0, 1,\ldots, i,\ldots, L, L+1\}$.
H_k	set of indices of potential targets visited by UAV k, $H_k=\{h,\ldots, i,\ldots, j\}$; $h,i,j \in \mathbf{T}, k \in \mathbf{U}$.
v	flight speed of a UAV.
T_{max}	maximum travel time of a UAV.
w_i	weight of a potential target i, $i \in \mathbf{T}$.
p	detection-error probability of a sensor carried by a UAV, $p \in (0,1)$.
d_{ij}	distance between points i and j, $i,j \in \mathbf{A}$.
t_{ij}	travel time between points i and j, $i,j \in \mathbf{A}$.
$t^k_{0(L+1)}$	total mission execution time of UAV k, $k \in \mathbf{U}$.
x^k_{ij}	binary variable representing whether UAV k travels from point i and j, $k \in \mathbf{U}$, $i,j \in \mathbf{A}$.

Based on an analysis of the above cases, and in the case of limited UAV endurance, the RATAP could not only access potential targets with higher weights as much as possible, just like TOP, but it could also make multiple visits to potential targets to make full use of the sustainability of a UAV. As a result, the probability of the successful collection of information from potential targets increased, and the expected reward of rapid-assessment tasks was correspondingly maximized. In the next section, we describe RATAP and specify its mathematical model.

III. RAPID-ASSESSMENT TASK-ASSIGNMENT PROBLEM (RATAP)

In the RATAP, the expected reward of a task-allocation scheme is not only related to the detection error probability of the sensor carried by the UAV but also to the weight of the potential target and the number of times it is accessed. The locations and weights of all potential targets are known. Table 1 lists the relevant indices, sets, parameters, and variables used in this paper.

A. UNMANNED AERIAL VEHICLES

$\mathbf{U}$ denotes the set of K UAVs performing rapid-assessment tasks. Since UAVs owned by same rescue agency are usually the same, we assumed that all the UAVs are homogeneous, i.e., the endurance of the UAVs and the detection-error probability of the sensors carried by the UAVs are the same and are known. All the UAVs start from the same starting point and return to the same destination after completing the rapid-assessment task. By considering the characteristics of the UAVs performing the rapid-assessment task, we assume that the UAVs have the ability to avoid obstacles automatically, could perform rapid-assessment tasks safely, and that the resulting path deviation from the total flight path length is very small and can be ignored.

B. POTENTIAL TARGETS

The start and end depots of the UAV are represented by 0 and $L+1$, respectively. The set $\mathbf{T}=\{1, 2, \ldots, i, \ldots, L\}$ consists of the L potential targets to be visited in the earthquake-stricken region. The set of all points is $\mathbf{A}=\{0, 1, \ldots, i, \ldots, L, L+1\}$. The weight of a potential target is represented by $w_i \in \{1, 2, \ldots, 10\}$. The greater the weight is, the more important the target is, and the greater the weight points from the UAV access point are, the greater its expected reward is.

The decision variable x^k_{ij} is used: $x^k_{ij}=1$ if UAV k leaves target i and flies directly to target j without passing through any other targets, otherwise $x^k_{ij}=0$ was used. The number of times y_i that the potential target i is visited is calculated as follows:

$$y_i=\sum_{k=1}^{K}\sum_{j=1}^{L+1}x^k_{ij}, \quad i \in \mathbf{T}. \tag{1}$$

C. TASK EXECUTION TIME OF UAV

The set $H_k=\{h, \ldots, i, \ldots, j\}$; $h, i, j \in T, k \in U$, is used to represent the path of UAV k that performs a rapid-assessment task. Since all UAVs must start from the starting point and return to the same destination, H_k omits the number of start and end points. The travel time between point i and point j is calculated as follows:

$$t_{ij}=\frac{d_{ij}}{v}, \quad \forall i,\ j \in \mathbf{A}. \tag{2}$$

where d_{ij} is the Euclidean distance between points i and j, and v represents the flight speed of the UAV. The task execution time of UAV k is calculated as follows:

$$t^k_{0(L+1)}=\sum_{i=0}^{L}\sum_{j=1}^{L+1}x^k_{ij}t_{ij}. \tag{3}$$

D. EFFECTIVENESS OF RAPID-ASSESSMENT TASK

In this paper, the expected reward is used to quantitatively represent the effectiveness of the multi-UAV rapid-assessment task, which is related to the weight w_i of the potential target, i, and the detection-error probability, p, of a sensor carried by a UAV. The expected benefit of multi- UAVs performing one quick-assessment task on target i is calculated

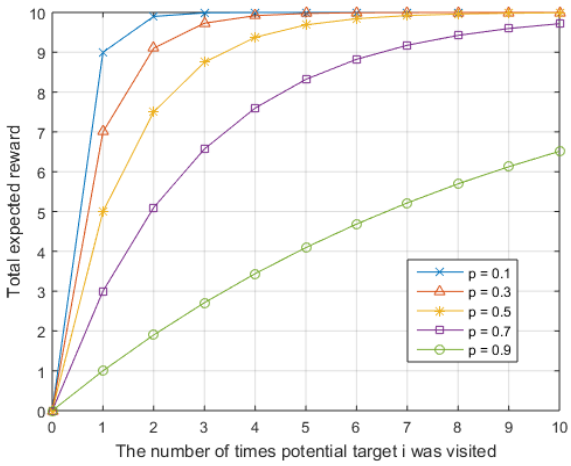

FIGURE 3. Trend of total expected return R_i with the number of times target i was visited y_i with a fixed weight $w_i = 10$ and different detection-error probability p.

as follows:

$$R_i = w_i \cdot (1 - p). \tag{4}$$

As has been reported previously [36], the probability of successful collection by other UAVs is not dependent on whether a UAV collects the information from a potential target. Therefore, the total expected reward after y_i visits to potential target i is calculated as follows:

$$R_i = w_i \cdot (1 - p^{y_i}), \tag{5}$$

where the weight w_i of potential target i and detection-error probability p of the sensor are both known.

Fig. 3 shows the trend as the total expected reward. R_i increased with the number of times target i is visited, y_i, with a fixed weight, $w_i = 10$, but different detection-error probability, p. This is the most important difference between the TOP, under which the reward from each accessed target is fixed, and the RATAP.

E. MATHEMATICAL MODEL

To solve the problem of a multi-UAV rapid-assessment task-assignment after an earthquake, we design the objective function in this work to maximize the total expected reward of the task-assignment scheme. The mathematical model is formulated with the two decision variables: $x_{ij}^k = 1$ if UAV k leaves target i and flies directly to target j without passing through any other targets, and $x_{ij}^k = 0$ otherwise; $y_i =$ the number of times that potential target i is visited. The model is as follows:

$$Max \quad \sum_{i=1}^{L} w_i \left(1 - p^{y_i}\right), \tag{6}$$

$$S.t.: \quad \sum_{i=1}^{L} x_{0\,i}^k = \sum_{j=1}^{L} x_{j(\mathrm{L}+1)}^k = 1; \quad \forall k \in \mathbf{U}, \tag{7}$$

$$\sum_{h=0}^{L} x_{hi}^k = \sum_{j=1}^{L+1} x_{ij}^k; \quad \forall i \in \mathbf{T},\ k \in \mathbf{U}, \tag{8}$$

$$\sum_{i=0}^{L} \sum_{j=1}^{L+1} t_{ij} x_{ij}^k \le T_{\max}; \quad \forall k \in \mathbf{U}, \tag{9}$$

$$x_{ij}^k \in \{0, 1\}; \quad \forall i,\ j \in \mathbf{T},\ k \in \mathbf{U}. \tag{10}$$

The objective function (6) is to maximize the expected reward of the rapid-assessment task-scheme. Constraint (7) guarantees that any UAV k in the set $\mathbf{U}$ must begin at the starting point and return to the end point. Constraint (8) is the path connectivity constraint, which requires that for any UAV k in the set $\mathbf{U}$, the in-degree of target i is equal to the out-degree. Constraint (9) guarantees that the duration of the mission performed by any UAV k in the set $\mathbf{U}$ is less than or equal to its maximum endurance. Constraint (10) involves the values of the binary decision variables: $x_{ij}^k = 1$ if UAV k leave target i and flies directly to target j without passing through any other targets, and $x_{ij}^k = 0$ otherwise.

IV. HYBRID PARTICLE SWARM OPTIMIZATION WITH SIMULATED ANNEALING (HPSO-SA) ALGORITHM

The HPSO-SA algorithm consists of two layers of loops, that combined the PSO and SA appropriately. The simulated annealing operation is carried out in the external loop, and the internal loop performs a particle update operation. The algorithm framework combines the fast convergence of the PSO [37] and the strong local optimization of the SA [38]. The pseudocode of the HPSO-SA algorithm is shown in Table 2.

The algorithm starts with an initial particle swarm and set an initial temperature. Each particle x records its current position, $S[x].pos$, and the known optimal position, $S[x].lbest$, after which time the particle updated its position during the iteration and gradually approaches the global optimal position, $S[best].lbest$. Then, the simulated annealing operation is used to optimize $S[best].lbest$ by locally searching for it in each iteration. If an improvement is made, the global optimal particle $S[best].lbest$ is updated and returns to the PSO for the next iteration. A cooling operation is then implemented according to the established cooling strategy after each iteration is complete until the temperature fell below the predetermined termination temperature. At that point, the algorithm is terminated, and $S[best].lbest$ is the optimal solution to the problem. Through multiple rounds of interaction between the PSO and SA, the algorithm combines the fast convergence characteristics of the PSO and strong local optimization of the SA. Table 3 lists the parameters related to the HPSO-SA algorithm in this paper.

The computational complexity of an algorithm is dependent mainly on its structure and implementation. The HPSO-SA algorithm mainly consists of an evaluation and update of PSO particles and an improvement of the best particle through SA iterations. We let N_{Ex} be the number of external loops and N_P be the length of the particle.

TABLE 2. Pseudocode of the HPSO-SA algorithm.

Input: S a swarm of N_S particles;

Output: $S[best].lbest$ best position found;

```
1   initialize parameters of HPSO-SA Algorithm;
2   position each particle in S (see Section 4.1);
3   evaluate S and update S[x].lbest & S[best].lbest (see Section 4.2) ;
4   while T^iter > T_end
5       foreach x in [1…N_S] do
6           update S[x].pos (see Section 4.3);
7       endfor
8       evaluate S and update S[x].lbest & S[best].lbest;
9       improve S[best].lbest through SA iteration (see Section 4.4);
10      if S[best].lbest improved then
11          update S[best].lbest;
12      endif
13      T^iter = T^iter * R_T
14  endwhile
```

TABLE 3. Parameters related to the HPSO-SA algorithm.

Notation	Explanation
N_S	the particle swarm size
ω	inertial coefficient, reflects the tendency of particles to maintain their current state
c_1	cognitive factor, reflects the trends of the approach to the local optimum
c_2	social factor, reflects the trends of the approach to the global optimum
r_1	random number generated in the interval (0,1)
r_2	random number generated in the interval (0,1)
N_{SA}	the number of SA operations
T_0	initial temperature of SA operations
T_{END}	termination temperature of SA operations
R_T	cooling rate of SA operations, positive but less than 1

Indices of potential targets	3	4	1	4
Indices of UAVs	1	1	2	2

FIGURE 4. An example of particle encoding method of the HPOS-SA algorithm.

According to the design of the HPSO-SA algorithm, $N_{Ex} = \left\lceil \frac{\log T_{END} - \log T_0}{\log R_T} \right\rceil$. Because the target is allowed to be revisited, $N_P = T_{\max} \times L \times K$ in the worst case. Since the algorithm-related parameters, such as N_S, N_{SA}, T_0, T_{END}, R_T, and N_{Ex}, are preset, that is, they do not change with the scale of the problem, they can be regarded as constants when performing the algorithm analysis. The complexity of the HPSO-SA algorithm depends on the steps shown in lines 2, 3, 6, 8, and 9 in Table 3. The complexity of each step is analyzed as follows:

(1) The complexity of line 2 is $O(N_P \times N_S) \approx O(N_P)$.

(2) The complexity of line 3 is $O(N_P \times N_S + \mathrm{N}_S \times logN_S) \approx O(N_P)$.

(3) The complexity of line 6 is $O(N_{Ex} \times N_S \times N_P \times \log N_P) \approx O(N_P \times \log N_P)$.

(4) The complexity of line 8 is $O(N_{Ex} \times (N_P \times N_S + N_S \times logN_S)) \approx O(N_P)$.

(5) The complexity of line 9 is $O(N_{Ex} \times (N_{SA} \times N_P \times \log N_P)) \approx O(N_P \times \log N_P)$.

Above all, the complexity of the HPSO-SA algorithm is $O(N_P \times \log N_P) \approx O(L \times K \times \log(L \times K))$.

A. PARTICLE SWARM INITIALIZATION

In the HPSO-SA algorithm, the position of each particle represents a feasible solution of the RATAP. The indices of the potential target and the UAV are the two basic units of the particles, which are integers. The first line of particles is composed of the indices of the potential targets that are visited by a UAV, and the second line of particles is the index of the UAV.

The particle code in Fig. 4 indicates that UAV1 begins at the starting point, accesses potential target 3, accesses potential target 4, and returns to the end point. UAV2 begins at the starting point, accesses potential target 1, accesses potential target 4, and returns to the end point.

Based on the above encoding rules, the initialization of the particle swarm is completed using the following five steps:

Step 1: A "T_{max} *ellipse*" is constructed using the starting and ending points as the two foci of the ellipse and the UAV endurance T_{max} as the length of the major axis [39], [40]. The indices of potential targets corresponding to the point outside "T_{max} *ellipse*" are deleted from set **T** to obtain set **T'**. The specific implementation is as follows. We calculate the sum of the distances from each target in the set **T** to the starting point and ending point. We find out the indices corresponding to the potential targets, whose cumulative distance is greater than T_{max}. Then, we delete these indices from the set **T** to obtain set **T'**.

Step 2: The indices of the potential targets in set **T'** are randomly arranged to obtain a task-execution path of UAV k, which is represented as H_k.

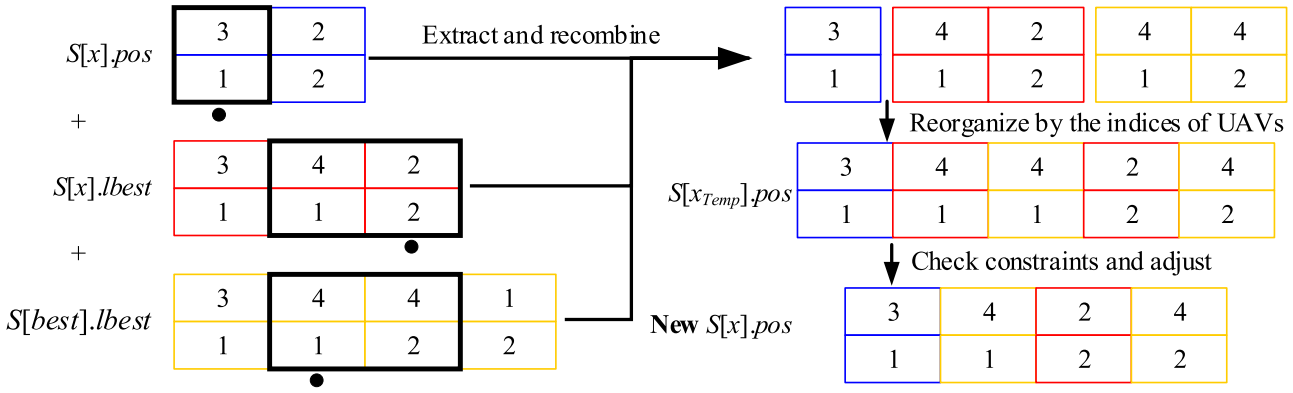

FIGURE 5. An example of a particle-update operation.

Step 3: The task execution time of UAV k, $t^k_{0(L+1)}$, is calculated based on H_k. If $t^k_{0(L+1)} > T_{\max}$, then random deletion of a target index in H_k is executed and repeated until a feasible path of UAV k is obtained. If H_k is empty after a random deletion operation, the algorithm returns to Step 2 to regenerate H_k.

Step 4: Steps 2 and 3 are repeated based on the number of UAVs until all UAVs have a feasible task-assignment scheme. The feasible path of all UAVs is taken as the first line of particles, and the index of corresponding UAV k is taken as the second line of particles to obtain an initial particle.

Step 5: The initial particle swarm is obtained by repeating Steps 2–4 according to the preset particle-swarm size.

B. PARTICLE EVALUATION AND OPTIMAL PARTICLE UPDATE OPERATION

The particles in the HPSO-SA algorithm have positions but no velocity vectors. The position of one particle represents a task-allocation scheme for the rapid assessment of multiple UAVs. The fitness of particles represents the expected reward of the task-allocation scheme. Thus, Equation (6) is selected as the fitness function of the algorithm. A greater particle fitness corresponds to a higher expected reward of the task-allocation scheme that the particle represents.

Every time a particle-update operation is completed, the optimal particle is updated. The process is as follows. The fitness *Fit[x].pos* of the current position *S[x].pos* of particle x is calculated. If *Fit[x].pos* is better than the fitness *Fit[x].lbest*, which represents the known optimal position *S[x].lbest*, then *S[x].lbest*is replaced with *S[x].pos* and *Fit[x].lbest* is replaced with *Fit[x].pos*. Similarly, if *Fit[x].pos* is better than the global optimal position *S[best].lbest* fitness *Fit[best].lbest*, then *S[best].lbest* is replaced with *S[x].pos* and *Fit[best].lbest* is replaced with *Fit[x].pos*. If the above conditions are not met, the optimal particles are not updated.

C. PARTICLE UPDATE OPERATION

The particle-update operation updates the position of particle x through the recombination of the three particles *S[x].pos*, *S[x].lbest*, and *S[best].lbest*. There are many types of recombination operators [41]. We propose a new recombination operator based on the core idea of extracting a part of each of the particles of *S[x].pos*, *S[x].lbest*, and *S[best].lbest*. The new particle is obtained by combining the three parts in order.

The lengths of *S[x].pos*, *S[x].lbest* and *S[best].lbest* are denoted as N_x, N_{xl} and N_{bl}, respectively. The numbers of the target indices extracted from these particles are $\omega \cdot N_x$, $(1-\omega)\cdot c_1 \cdot r_1 \cdot N_{xl}$, and $(1-\omega)\cdot c_2 \cdot r_2 \cdot N_{bl}$, respectively. All the calculation results are rounded up to the next integer, and the starting position of particle extraction is randomly generated. Fig. 5 shows an example of a particle-update operation. Letting $\omega = 0.5$, $c_1 = 1.8$, $c_2 = 1.6$, $r_1 = 0.6$ and $r_2 = 0.4$, then the numbers of target indices extracted from S[x].pos, S[x].lbest and S[best].lbest can be calculated as: $\omega \cdot N_x = 1$, $(1-\omega)\cdot c_1 \cdot r_1 \cdot N_{xl} = 2$ and $(1-\omega)\cdot c_2 \cdot r_2 \cdot N_{bl} = 2$, respectively. Supposing that the randomly generated particle extracting position are 1, 3, 2, respectively, then the recombination process of a new particle is as follows: Starting from the first position, one bit is extracted from the *S[x].pos* particle; from the third position, two bits are extracted from the *S[x].lbest* particle; from the second position, two bits are extracted from the *S[best].lbest* particle; and a new particle is recombined. After being reorganized by the indices of UAVs, $S\left[x_{Temp}\right].pos$ is obtained.

The position $S\left[x_{Temp}\right].pos$ shown in Fig. 5 of temporary particle x_{Temp}, which is produced by the update operation (extract, recombine and reorganize) does not necessarily satisfy the constraints of the RATAP model. Therefore, it is necessary to perform constraint-checks and adjustments on the particles that do not satisfy the constraints. Path-connectivity verification and endurance verification on the particles have to be performed according to Equations (8) and (9), respectively. We refer to particles that do not satisfy Equation (8) as Violator A types, particles that do not satisfy Equation (9) as Violator B types, and particles that do not satisfy Equations (8) and (9) simultaneously as Violator C types. The $S\left[x_{Temp}\right].pos$ shown in Fig. 5 is a Violator A type.

In view of the above three types of violation particles, the following three particle-adjustment strategies are designed:

Adjustment Strategy 1: For Violator A, the duplicate target indices are deleted, as shown in Fig 5.

Adjustment Strategy 2: For Violator B, the indices of the particles with the lowest weights are deleted sequentially until the endurance constraints are satisfied.

Adjustment Strategy 3: For Violator C, the duplicate target indices are deleted first, and then the indices of the particles with the lowest weights are deleted sequentially until the endurance constraints are satisfied.

A particle obtained after constraint check and adjustment is a feasible solution of the RATAP.

D. THE OPERATION OF SIMULATED ANNEALING

In the operation of simulated annealing, a local search strategy is used to optimize the global optimal particle, *S[best].lbest*, which is obtained through a particle update operation. The most important characteristic of SA is the probability jump-out, which is called the metropolis process [42]. Researchers have proven the theory that SA can converge to the global optimum with a probability of approximately 1 by controlling the cooling process [43], [44].

In the RATAP, task-assignment schemes with the same expected reward may have different access orders of potential targets. By optimizing the path lengths of the task-allocation schemes with the same expected reward, the flight distance of a UAV can be shortened. Thus, more potential targets can be accessed, and the expected reward of a task-assignment scheme can be improved. In this paper, the following four disturbance strategies are designed.

Disturbance Strategy 1: Two-point exchange. Two particle positions are randomly selected for exchange.

Disturbance Strategy 2: Reverse the order between two points. Two particle positions are randomly selected and the particles between them are arranged in reverse order.

Disturbance Strategy 3: Delete a target index. One particle position is randomly selected, and the target index and UAV index on it are deleted.

Disturbance Strategy 4: Insert a target index. One particle position is randomly selected and a new target index is inserted. If all the target indices are included, the target index with the largest weight is inserted.

In each round of a simulated annealing operation, one of the above four disturbance strategies is randomly selected to generate a new solution. We used the method in Section IV-C to perform the constraint checks and adjustment on the new particle, and a new solution that satisfied all the constraints is obtained. Finally, a new solution is received with a certain probability using the metropolis criterion.

V. EXPERIMENT AND ANALYSIS

In the experiment described in Section V-A, we use two sets of benchmark instances of the TOP model for algorithm testing. For the analysis conducted in Section V-B, for the characteristics of the post-earthquake rapid-assessment task, we generate 18 simulation cases to demonstrate the performance of the HPSO-SA algorithm. The optimal parameter settings of the algorithm we settled on are described in Section V-C.

All the experiments are conducted in an environment of an i5-6500 CPU 3.2-GHz, 8-GB desktop computer and in MATLAB R2015a. The initial parameters of the HPSO-SA algorithm are as follows:

(1) For particle swarm size, $N_S = 50$ particles.

(2) For the inertial coefficient ω, which reflects the tendency of particles to maintain their current state, $\omega = 0.5$.

(3) The cognitive factor c_1 and social factor c_2 reflect the trends of the approach to the local and global optimum, respectively; $c_1 = 1.8$ and $c_2 = 1.6$. r_1 and r_2 are random numbers between 0 and 1.

(4) For initial temperature $T_0 = 100$, termination temperature $T_{END} = 1$, and cooling rate $R_T = 0.9$.

(5) For number of annealing times $N_c = 50$ times.

A. NUMERICAL EXPERIMENT

In the RATAP problem, if the sensor-detection error probability is 0, and the potential target is accessed at most once, it can be converted to a TOP problem. Thus, we select 18 TOP model benchmark instances [39] to test the model and algorithm proposed in this paper. The dataset is from https://www.mech.kuleuven.be/en/cib/op. These benchmark instances include seven groups, and the numbers of vertices, N, of these groups were 32, 21, 33, 100, 66, 64, and 102. In all instances of the same group, the position and weight of the vertices were constant, but the maximum duration, $T_{\max}$, of a UAV was different, and the UAV number, K, increased from 2 to 4.

First, we select 18 benchmark instances with maximum endurances of $T_{\max} = 20$ for the seven types of datasets to test the performance of the HPSO-SA algorithm. Each instance is run 10 times under the same experimental conditions.

Table 4 shows the results of the solution of these 18 benchmark instances, where R_{MAX} represents the maximum reward of the 10 runs, CPU_{AVG} represents the average computational time in seconds of the 10 runs, and R_{BEST} represents the known optimal solution collected from [45]-[49]. The gap is calculated by $[(R_{BEST} - R_{MAX})/R_{BEST}] \times 100\%$, representing the relative difference between R_{MAX} and R_{BEST}. As shown in the experimental results in Table 4, under the same, $T_{\max}$, the HPSO-SA algorithm quickly and efficiently solves all seven types of TOP model benchmark instances. Among the 18 selected examples, the proposed algorithm obtains the optimal solution of 10 instances.

We further experimented with 32 instances of type 2 datasets with $N = 21$ to test the performance of the HPSO-SA algorithm. Each instance is run 10 times under the same experimental conditions. Table 5 shows the results of the solution of these 32 benchmark instances, where R_{MAX} represents the maximum reward of the 10 runs, CPU_{AVG} represents the average computational time in seconds of the 10 runs, and R_{BEST} represents the known optimal solution collected from [45]–[49]. As shown in the

TABLE 4. Results for the 18 benchmark instances.

Type	Instance	N	K	HPSO-SA		ACO		R_{BEST}*	Gap
				R_{MAX}	CPU_{AVG}	R_{MAX}*	CPU_{AVG}*		
1	p1.2.h	32	2	110	3.3	110	4.2	110	0.00%
	p1.3.l	32	3	155	4.7	155	5.6	155	0.00%
	p1.4.q	32	4	190	6.0	190	6.5	190	0.00%
2	p2.2.j	21	2	260	1.7	260	3.1	260	0.00%
3	p3.2.f	33	2	300	3.3	300	4.6	300	0.00%
	p3.3.j	33	3	360	4.9	380	5.8	380	5.26%
	p3.4.n	3	4	420	6.3	440	6.7	440	4.55%
4	p4.3.b	100	3	38	7.8	38	9.9	38	0.00%
	p4.4.d	100	4	38	10.9	38	12.2	38	0.00%
5	p5.2.h	66	2	385	3.8	410	9.6	410	6.10%
	p5.3.l	66	3	545	5.6	595	13.1	595	8.40%
	p5.4.p	66	4	690	6.8	760	16.3	765	9.80%
6	p6.2.f	64	2	534	4.1	588	9.9	588	9.18%
	p6.3.j	64	3	726	6.1	828	13.5	828	12.32%
	p6.4.n	64	4	810	10.8	1068	16.6	1068	24.16%
7	p7.2.b	102	2	64	5.8	64	8.6	64	0.00%
	p7.3.c	102	3	79	7.6	79	11.5	79	0.00%
	p7.4.d	102	4	79	9.3	79	14.1	79	0.00%

*: R_{MAX} and CPU_{AVG} of ACO were obtained from Reference [46], and R_{BEST} was obtained from Reference [45-49]

experimental results in Table 5, within the same dataset, the HPSO-SA algorithm quickly and efficiently solves all the instances. Among the 32 instances of type 2 datasets, the proposed algorithm obtains the optimal solution of all the instances.

The above two numerical experiments and the comparison with the ant colony optimization (ACO) algorithm in reference [46], demonstrate that although the RTOP-RP model and the HPSO-SA algorithm in this study were specifically designed for RATAP, for the small-scale TOP benchmark instances, the models and algorithms also obtains the optimal solution in a short period of time.

B. POST-EARTHQUAKE SIMULATION CASES

Since the characteristics of post-earthquake rapid-assessment tasks differ from the benchmark instances of the TOP, two types of datasets based on the distribution characteristics of potential targets after the earthquake are constructed: (1) a clustered distribution, which is shown in Fig. 6(a), and (2) an even distribution, which is shown in Fig. 6(b). The numbers of potential targets, N, of the two types of datasets are 13 and 23, respectively.

For the post-earthquake scenarios simulated through the above two types of datasets, K homogeneous UAVs are used to complete the rapid-assessment task. The number, K, of the UAV used to complete the rapid-assessment task increases from 2 to 4. Moreover, the values of the maximum safe endurance, $T_{\max}$, of the UAV were 10, 15 and 20 min, the flight speed is $v = 1$ km/min, and the probability of a detection error of the sensor carried by each drone is $p = 0.2$. The RATAP model is used to solve the problem, and the task-allocation scheme is used for rapid assessment after the

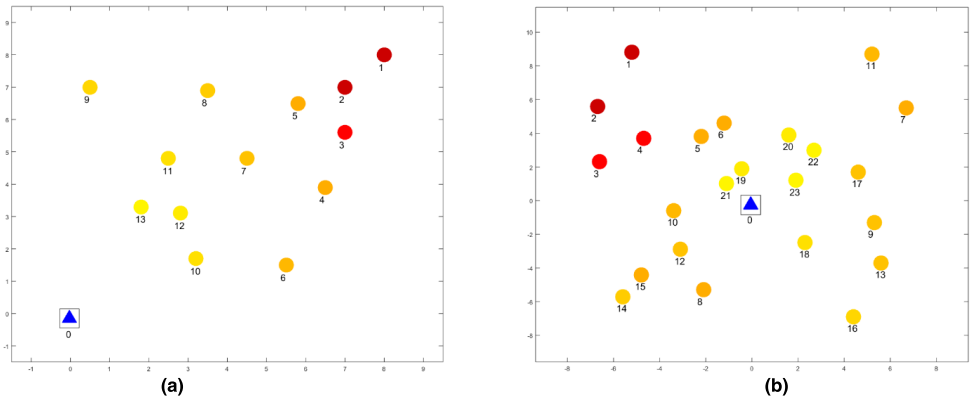

FIGURE 6. Dataset of two kinds of multi-UAV post-earthquake rapid-assessment tasks.

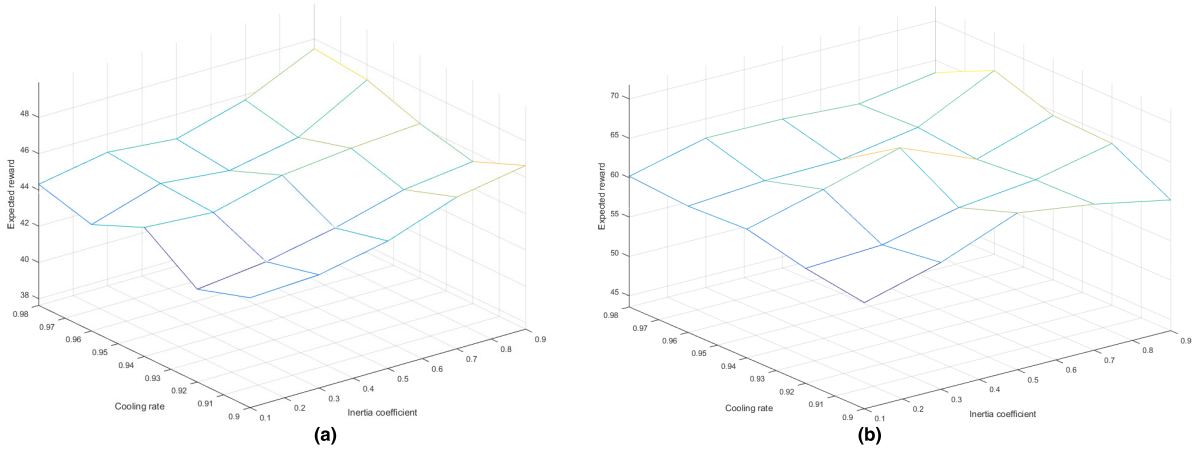

FIGURE 7. Expected reward under different particle inertia parameters and cooling rates.

earthquake is obtained. Each case is run 10 times under the same experimental conditions.

Table 6 shows the task-allocation schemes of the HPSO-SA for solving the 18 post-earthquake quick-assessment-task instances, where R_{MAX} represents the maximum reward of the 10 runs, R_{AVG} represents the average reward of the 10 runs,

R_{MIN} represents the minimum reward of the 10 runs, and CPU_{AVG} represents the average computational time in seconds of the 10 runs. As shown in Table 6, the stability of the HPSO-SA algorithm is very strong. The average gap between R_{MAX} and R_{AVG} is only 2.57%, and between R_{MAX} and R_{MIN}, it is only 4.95%.

C. ALGORITHM PARAMETER SETTING

By considering the influence of different parameter configurations on the performance of the heuristic algorithm, we further test the sensitivity of the algorithm parameters for the two types of datasets.

First, we consider the C-2-20 instance, as described in Section V-B. In the solution process of HPSO-SA, different inertia coefficients ω and cooling rates R_T are selected. The experimental results are shown in Table 7.

Furthermore, when we consider the E-2-20 instance, as described in Section V-B, in the solution process of the HPSO-SA algorithm, different inertia coefficients ω and cooling rates R_T are selected. The experimental results are shown in Table 8. From the above experimental results, it can be seen that for the C-type and E-type datasets, the HPSO-SA is generally stable in solving the RATAP, but the effect is different for different particle inertia parameters ω and cooling rates R_T, as shown in Fig. 7.

When the particle inertia parameter ω is fixed, the gain in the experiment generally exhibits an upward trend with an increase in the cooling rate, R_T, and the maximum gain is obtained when the inertia parameter, ω, is 0.5, and the cooling rate, R_T, is 0.94. When the cooling rate, R_T, is fixed, the gains in the experiment generally exhibits an upward trend with an increase in the inertia parameter, ω. Therefore, during the RATAP solution, the inertia parameter ω could be set to 0.5, and the cooling rate R_T could be set to 0.94.

VI. CASE STUDY

To illustrate the application of the above research work in real-life scenarios, we conducted a case study based on

TABLE 5. Results for the Type-2 benchmark.

Instance	N	K	T_{MAX}	HPSO-SA		ACO		R_{BEST}*
				R_{MAX}	CPU_{AVG}	R_{MAX}*	CPU_{AVG}*	
p2.2.a	21	2	7.5	90	2.0	90	2.0	90
p2.2.b	21	2	10	120	2.0	120	2.3	120
p2.2.c	21	2	11.5	140	1.9	140	2.5	140
p2.2.d	21	2	12.5	160	2.2	160	2.5	160
p2.2.e	21	2	13.5	190	2.0	190	2.7	190
p2.2.f	21	2	15	200	2.1	200	2.9	200
p2.2.g	21	2	16	200	2.0	200	3.0	200
p2.2.h	21	2	17.5	230	2.2	230	3.0	230
p2.2.i	21	2	19	230	2.2	230	3.1	230
p2.2.j	21	2	20	260	2.1	260	3.1	260
p2.2.k	21	2	22.5	275	2.3	275	3.2	275
p2.3.a	21	3	5	70	2.1	70	2.1	70
p2.3.b	21	3	6.7	70	2.5	70	2.3	70
p2.3.c	21	3	7.7	105	2.2	105	2.6	105
p2.3.d	21	3	8.3	105	2.4	105	2.6	105
p2.3.e	21	3	9	120	3.0	120	2.7	120
p2.3.f	21	3	10	120	2.9	120	2.8	120
p2.3.g	21	3	10.7	145	3.1	145	2.8	145
p2.3.h	21	3	11.7	165	2.9	165	3.0	165
p2.3.i.	21	3	12.7	200	2.8	200	3.2	200
p2.3.j	21	3	13.3	200	2.7	200	3.2	200
p2.3.k	21	3	15	200	2.6	200	3.3	200
p2.4.a	21	4	3.8	10	2.1	10	2.2	10
p2.4.b	21	4	5	70	2.6	70	2.6	70
p2.4.c	21	4	5.8	70	2.7	70	2.6	70
p2.4.d	21	4	6.2	70	2.5	70	2.6	70
p2.4.e	21	4	6.8	70	2.7	70	2.6	70
p2.4.f	21	4	7.5	105	2.7	105	2.9	105
p2.4.g	21	4	8	105	2.8	105	2.9	105
p2.4.h	21	4	8.8	120	2.9	120	3.0	120
p2.4.i	21	4	9.5	120	2.8	120	3.0	120
p2.4.j	21	4	10	120	2.9	120	3.0	120
p2.4.k	21	4	11.2	180	3.3	180	3.3	180

*: R_{MAX} and CPU_{AVG} of ACO were obtained from Reference [46], and R_{BEST} was obtained from Reference [45-49]

real data from the 2008 Wenchuan earthquake in China. On May 12, 2008, an earthquake of magnitude 8.0 hit Wenchuan, China. The epicenter was at 31.0°N, 103.4°E, and the focal depth was 14 km. The earthquake caused nearly 90,000 deaths or disappearances, along with the collapse of a large number of houses [50]. As the main body participating in post-disaster relief, the National Earthquake Response Support Service (NERSS) rushed to the disaster area to

TABLE 6. Experimental results of 18 post-earthquake rapid-assessment task instances.

Type	Instance	N	K	$T_{\max}$	R_{MAX}	R_{AVG}	R_{MIN}	CPU_{AVG}
C	C-2-10	12	2	10	5.76	5.76	5.76	3.01
	C-2-15			15	18.82	18.70	18.66	3.11
	C-2-20			20	45.44	43.29	39.27	3.98
	C-3-10		3	10	5.95	5.95	5.95	4.18
	C-3-15			15	22.05	22.02	21.89	4.94
	C-3-20			20	56.38	53.64	50.23	6.22
	C-4-10		4	10	5.99	5.99	5.99	5.40
	C-4-15			15	23.52	23.47	23.41	6.41
	C-4-20			20	59.49	57.92	55.93	8.26
E	E-2-10	23	2	10	15.74	15.74	15.74	3.00
	E-2-15			15	40.16	39.06	38.60	3.14
	E-2-20			20	59.36	53.76	51.72	3.90
	E-3-10		3	10	21.50	21.44	21.40	4.29
	E-3-15			15	52.16	49.99	48.61	4.57
	E-3-20			20	76.80	71.36	69.40	5.56
	E-4-10		4	10	27.16	27.15	27.14	5.69
	E-4-15			15	60.51	58.51	55.26	6.29
	E-4-20			20	86.30	81.12	74.07	7.36

conduct a rapid assessment of the disaster. Experts from relief agencies identified a number of potential targets that needed to be assessed rapidly based on known information, which included the latitude and longitude of important buildings such as schools and hospitals in the affected area. Combined with characteristics such as distance, population size, and building features, the weight of these potential targets was estimated. Thus, 50 potential targets were selected for case studies, as shown in Fig. 8.

Considering factors such as endurance and sensor specifications, the F-1000 fixed-wing UAV was used to perform the above post-disaster rapid-assessment task. The cruising speed of the UAV was 70 km/h. In consideration of the takeoff and landing, we assumed that the average speed of the UAV was 60 km/h. The maximum safe endurance of the UAV was 90 min. Considering the influence of uncertain factors (e.g., wind) on the endurance of the UAV, we assumed that the maximum safe endurance used to perform the task was 80 min. Moreover, a maximum of five UAVs could be used for the rapid-assessment task.

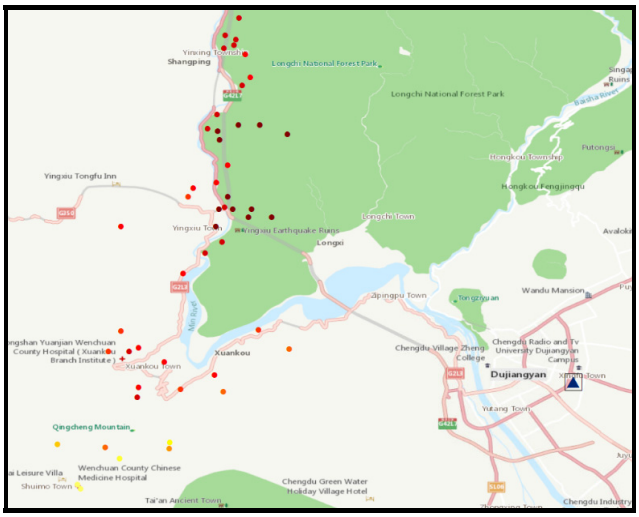

FIGURE 8. Potential targets of wenchuan earthquake and the location of the starting point of UAV.

We used the optimal parameter settings discussed in Section V-C to model the above rapid-assessment tasks using the RATAP model and solved them using the HPSO-SA algorithm. We assumed that the number of UAVs, K, used to complete the rapid-assessment task increased from three to five. The maximum safe endurance values, $T_{\max}$, of the UAV

TABLE 7. Expected rewards of C-2-20 for different inertia coefficients and cooling rates.

ω	R_T	Expected reward R		
		R_{MAX}	R_{AVG}	R_{MIN}
0.1	0.98	45.440	43.968	42.336
	0.96	45.440	44.291	40.480
	0.94	45.440	43.680	40.640
	0.92	45.440	43.398	39.584
	0.90	45.440	43.270	39.232
0.3	0.98	45.440	44.371	40.640
	0.96	45.440	44.240	40.640
	0.94	45.440	43.750	40.416
	0.92	45.440	43.334	39.840
	0.90	45.440	42.634	39.360
0.5	0.98	45.440	44.182	39.840
	0.96	45.440	43.942	40.640
	0.94	45.440	44.934	43.480
	0.92	45.440	44.134	42.560
	0.90	45.440	43.507	40.00
0.7	0.98	45.440	44.160	43.040
	0.96	45.440	44.592	40.480
	0.94	45.440	43.392	39.424
	0.92	45.440	43.491	39.840
	0.90	45.440	43.766	39.040
0.9	0.98	45.440	44.765	42.336
	0.96	45.440	44.397	42.336
	0.94	45.440	43.926	40.640
	0.92	45.440	43.021	39.232
	0.90	45.440	44.064	40.640

TABLE 8. Expected rewards of E-2-10 for different inertia coefficients and cooling rates.

ω	R_T	Expected reward R		
		R_{MAX}	R_{AVG}	R_{MIN}
0.1	0.98	59.680	56.435	49.760
	0.96	59.680	54.432	46.400
	0.94	59.360	54.196	49.440
	0.92	59.520	53.734	47.360
	0.90	59.680	51.584	47.200
0.3	0.98	59.680	56.560	47.680
	0.96	59.680	54.794	47.776
	0.94	59.680	55.146	47.520
	0.92	59.360	51.920	47.200
	0.90	59.200	53.766	49.600
0.5	0.98	59.680	55.734	48.320
	0.96	59.680	54.902	47.520
	0.94	59.680	56.800	49.760
	0.92	57.600	49.933	43.200
	0.90	59.680	54.925	47.520
0.7	0.98	59.680	54.848	49.760
	0.96	59.680	53.565	46.944
	0.94	59.360	53.638	44.512
	0.92	59.520	53.168	43.360
	0.90	59.360	54.669	49.760
0.9	0.98	59.680	54.074	45.600
	0.96	59.680	54.424	47.680
	0.94	59.680	54.934	46.944
	0.92	59.360	53.542	43.680
	0.90	59.360	51.712	47.808

were set to 60, 70 and 80 min. Nine cases were possible from the combination of K and $T_{\max}$, which were used to name each case. The results obtained by applying the HPSO-SA algorithm to solve the example cases are shown in Table 9. Specifically, Table 9 shows the number of access targets, N_{VT}, the number of revisited targets, N_{RT}, the expected benefit, R, of the rapid-assessment task, the algorithm runtime, CPU, the total task execution time, T_E, of the UAVs performing rapid-assessment tasks, and the utilization rate, R_U, of UAVs' endurance.

Analyzing the results of the case study, we found the following:

(1) A UAV revisited potential targets with higher weights as much as possible. In all nine cases, more than 80% of the potential targets with weights of 10 were revisited. In particular, in the (5, 80) case, all targets with a weight of 10 were revisited. The experimental results verified that the RATAP model proposed in this paper could improve the effectiveness of a multi-UAV rapid-assessment task after an earthquake.

TABLE 9. Results of case examples.

Case	N_{VT}	N_{RT}	R	CPU	T_E	R_U
(3, 60)	34	21	280.69	6.43	179.79	99.89%
(3 70)	37	26	304.53	7.20	209.93	99.97%
(3, 80)	47	33	357.29	7.65	239.66	99.86%
(4, 60)	38	28	311.33	8.41	239.80	99.92%
(4, 70)	42	31	338.25	8.50	279.69	99.89%
(4, 80)	47	36	361.61	9.27	319.80	99.94%
(5, 60)	43	32	350.94	10.99	299.46	99.82%
(5, 70)	44	35	353.39	11.44	349.64	99.90%
(5, 80)	47	39	369.31	11.05	399.55	99.89%

(2) The total task-execution time of the rapid assessment almost reached the upper limit of the endurance of the UAVs. In all nine cases, the total task execution time accounted for more than 99.8% of the UAVs' total endurance capacity. It was also verified that the RATAP model could maximize a UAV's endurance and avoid wasting valuable rescue resources.

(3) The HPSO-SA algorithm could obtain high-quality multi-UAV task-allocation schemes in a short period of time. In all nine cases, the algorithm ran for no more than 12 s. In time-critical post-disaster relief operations, it is valuable to obtain a better task-allocation solution quickly than to obtain an optimal solution.

VII. CONCLUSION AND FUTURE WORK

In this study, a multi-UAV task-allocation method for rapid-assessment tasks in post-earthquake scenarios was studied. Based on the constraints of the UAV endurance and detection-error probability of the sensors carried by UAVs, a multi-UAV revisit-allowed task-assignment strategy was proposed, and a problem called the rapid-assessment task-assignment problem (RATAP) was introduced and defined using the RTOP-RP model. The optimization objective of the model was to maximize the expected reward of the rapid-assessment task scheme, allowing the target to obtain an expected reward with a certain probability when it was revisited. In this regard, we also specifically designed the HPSO-SA algorithm which combined the fast convergence characteristics of the PSO and strong local optimization of the SA to solve RTOP-RP model. The experimental results showed that the HPSO-SA could obtain a high-quality task-allocation scheme in a relatively short period of time. In future research, the rapid assessment task of area targets that were potential targets with large areas that could not be regarded as point targets will be further considered. An area target is sufficiently large that a UAV must fly back and forth within the area to collect information. After completing the information-collection task for an area target, a UAV flies to the next area target. Thus, integrated area-coverage mode optimization and path optimization between area targets must be considered in a multi-UAV rapid-assessment task-assignment problems for area targets.

ACKNOWLEDGMENT

The authors wish to thank LetPub (www.LetPub.com) for its linguistic assistance during the preparation of this manuscript. We also thank the editor and anonymous referees for their helpful comments for improving the quality of this paper.

REFERENCES

[1] (2009). *Global Assessment Report*. Accessed: Oct. 23, 2018. [Online]. Available: https://www.preventionweb.net/english/hyogo/gar/2009/?Atlas2017

[2] (2011). *Global Assessment Report on Disaster Risk Reduction*. Accessed: Oct. 23, 2018. [Online]. Available: https://www.preventionweb.net/english/hyogo/gar/2011/en/home/index.html

[3] (2013). *Global Assessment Report on Disaster Risk Reduction*. Accessed: Oct. 23, 2018. [Online]. Available: https://www.preventionweb.net/english/hyogo/gar/2013/en/home/index.html

[4] (2015). *Global Assessment Report on Disaster Risk Reduction*. Accessed: Oct. 23, 2018. [Online]. Available: https://www.preventionweb.net/english/hyogo/gar/2015/en/home/

[5] (2017). *The Atlas—Unveiling Global Disaster Risk*. Accessed: Oct. 23, 2018. [Online]. Available: https://www.preventionweb.net/english/hyogo/gar/atlas/download.html

[6] (2017). *Global Risks Report*. Accessed: Oct. 23, 2018. [Online]. Available: http://reports.weforum.org/global-risks-2017
[7] B. E. Oruc and B. Y. Kara, "Post-disaster assessment routing problem," *Transp. Res. B, Methodol.*, vol. 116, pp. 76–102, Oct. 2018.
[8] T. K. Šipoš and M. Hadzima-Nyarko, "Rapid seismic risk assessment," *Int. J. Disaster Risk Reduction*, vol. 24, pp. 348–360, Sep. 2017.
[9] S. Zhang, K. Yang, and Y. Cao, "GIS-based rapid disaster loss assessment for Earthquakes," *IEEE Access*, vol. 7, pp. 6129–6139, 2018.
[10] A. Nadi and A. Edrisi, "Adaptive multi-agent relief assessment and emergency response," *Int. J. Disaster Risk Reduction*, vol. 24, pp. 12–23, Sep. 2017.
[11] T. Feng, Z. Hong, H. Wu, Q. Fu, C. Wang, C. Jiang, and X. Tong, "Estimation of Earthquake casualties using high-resolution remote sensing: A case study of Dujiangyan city in the May 2008 Wenchuan Earthquake," *Natural Hazards*, vol. 69, no. 3, pp. 1577–1595, Dec. 2013.
[12] D. Giordan, Y. Hayakawa, F. Nex, F. Remondino, and P. Tarolli, "Review article: The use of remotely piloted aircraft systems (RPASs) for natural hazards monitoring and management," *Natural Hazards Earth Syst. Sci.*, vol. 18, no. 4, pp. 1079–1096, Apr. 2018.
[13] D. Giordan, A. Manconi, F. Remondino, and F. Nex, "Use of unmanned aerial vehicles in monitoring application and management of natural hazards," *Geomatics, Natural Hazards Risk*, vol. 8, no. 1, pp. 1–4, May 2017.
[14] D. Floreano and R. J. Wood, "Science, technology and the future of small autonomous drones," *Nature*, vol. 521, no. 7553, pp. 460–466, May 2015.
[15] F. Zhou, Y. Wu, R. Q. Hu, and Y. Qian, "Computation rate maximization in UAV-enabled wireless-powered mobile-edge computing systems," *IEEE J. Sel. Areas Commun.*, vol. 36, no. 9, pp. 1927–1941, Sep. 2018.
[16] T. Zeng, W. Yang, H. Wu, "UAV remote sensing image processing and classification in Wenchuan Earthquake district," *Proc. SPIE*, vol. 7498, Oct. 2009, Art. no. 749823.
[17] H. Jiang, Y. Su, Q. Jiao, J. Zhang, G. Lixia, and Y. Luo, "Typical geologic disaster surveying in Wenchuan 8.0 Earthquake zone using high resolution ground LiDAR and UAV remote sensing," *Proc. SPIE*, vol. 9262, Nov. 2014, Art. no. 926219.
[18] D. Dominici, M. Alicandro, and V. Massimi, "UAV photogrammetry in the post-Earthquake scenario: Case studies in L'Aquila," *Geomatics, Natural Hazards Risk*, vol. 8, no. 1, pp. 87–103, May 2017.
[19] D. Duarte, F. Nex, N. Kerle, and G. Vosselman, "Towards a more efficient detection of earthquake induced facade damages using oblique UAV imagery," in *Proc. Int. Arch. Photogram., Remote Sens. Spatial Inf. Sci.*, Bonn, Germany, vol. XLII-2/W6, 2017, pp. 93–100.
[20] C. Corbane, K. Saito, L. Dell'Oro, E. Bjorgo, S. P. Gill, B. Emmanuel Piard, C. K. Huyck, T. Kemper, G. Lemoine, R. J. Spence, and R. Shankar, "A comprehensive analysis of building damage in the 12 January 2010 Mw7 haiti Earthquake using high-resolution satelliteand aerial imagery," *Photogramm. Eng. Remote Sens.*, vol. 77, no. 10, pp. 997–1009, Oct. 2011.
[21] R. R. Murphy, "Marine heterogeneous multirobot systems at the great Eastern Japan Tsunami recovery," *J. Field. Robot.*, vol. 29, no. 5, pp. 819–831, Oct. 2012.
[22] Z. Xu, J. Yang, C. Peng, Y. Wu, X. Jiang, R. Li, Y. Zheng, Y. Gao, S. Liu, and B. Tian, "Development of an UAS for post-Earthquake disaster surveying and its application in Ms7.0 Lushan Earthquake, Sichuan, China," *Comput. Geosci.*, vol. 68, pp. 22–30, Jul. 2014.
[23] K. W. Franke, K. M. Rollins, C. Ledezma, J. D. Hedengren, D. Wolfe, S. Ruggles, C. Bender, and B. Reimschiissel, "Reconnaissance of two liquefaction sites using small unmanned aerial vehicles and structure from motion computer vision following the April 1, 2014 chile Earthquake," *J. Geotech. Geoenviron. Eng.*, vol. 143, no. 5, pp. 04016125-1–04016125-11, May 2017.
[24] A. Saffarzadeh, T. Shimaoka, H. Nakayama, T. Hanashima, K. Yamaguchi, and K. Manabe, "Tasks and problems involved in the handling of disaster waste upon April 2016 Kumamoto Earthquake, Japan," *Natural Hazards*, vol. 89, no. 3, pp. 1273–1290, Dec. 2017.
[25] M. Y. Arafat and S. Moh, "Location-aided delay tolerant routing protocol in UAV networks for post-disaster operation," *IEEE Access*, vol. 6, pp. 59891–59906, 2018.
[26] S. D. Ramchurn, T. D. Huynh, F. Wu, Y. Ikuno, J. Flann, L. Moreau, J. E. Fischer, W. Jiang, T. Rodden, E. Simpson, S. Reece, S. Roberts, and N. R. Jennings, "A disaster response system based on human-agent collectives," *J. Artif. Intell. Res.*, vol. 57, pp. 661–708, Dec. 2016.
[27] W. J. Gutjahr and P. C. Nolz, "Multicriteria optimization in humanitarian aid," *Eur. J. Oper. Res.*, vol. 252, no. 2, pp. 351–366, Jul. 2016.
[28] A. Otto, N. Agatz, J. Campbell, B. Golden, and E. Pesch, "Optimization approaches for civil applications of unmanned aerial vehicles (UAVs) or aerial drones: A survey," *Networks*, vol. 72, no. 4, pp. 411–458, Mar. 2018.
[29] S. Trigui, A. Koubâa, O. Cheikhrouhou, B. Qureshi, and H. Youssef, "A clustering market-based approach for multi-robot emergency response applications," in *Proc. IEEE Int. Conf. Auto. Robot Syst. Competitions*, Braganca, Portugal, May 2016, pp. 137–143.
[30] M. Cannioto, A. D'Alessandro, G. Lo Bosco, S. Scudero, and G. Vitale, "Brief communication: Vehicle routing problem and UAV application in the post-Earthquake scenario," *Natural Hazards Earth Syst. Sci.*, vol. 17, no. 11, pp. 1939–1946, Nov. 2017.
[31] M. Huang, K. Smilowitz, and B. Balcik, "Models for relief routing: Equity, efficiency and efficacy," *Transp. Res. E, logistics Transp. Rev.*, vol. 48, no. 1, pp. 2–18, Jan. 2012.
[32] B. Balcik, "Site selection and vehicle routing for post-disaster rapid needs assessment," *Transp. Res. E, Logistics Transp. Rev.*, vol. 101, pp. 30–58, May 2017.
[33] M. Huang, K. R. Smilowitz, and B. Balcik, "A continuous approximation approach for assessment routing in disaster relief," *Transp. Res. B, Methodol.*, vol. 50, pp. 20–41, Apr. 2013.
[34] V. Mersheeva and G. Friedrich, "Routing for continuous monitoring by multiple micro UAVs in disaster scenarios," in *Proc. 20th Eur. Conf. Artif. Intell.*, Montpellier, France, 2012, pp. 588–593.
[35] J. Al Hage, M. E. El Najjar, and D. Pomorski, "Multi-sensor fusion approach with fault detection and exclusion based on the Kullback–Leibler Divergence: Application on collaborative multi-robot system," *Inf. Fusion*, vol. 37, pp. 61–76, Sep. 2017.
[36] Y. Xia, R. Batta, and R. Nagi, "Controlling a fleet of unmanned aerial vehicles to collect uncertain information in a threat environment," *Oper. Res.*, vol. 65, no. 3, pp. 674–692, Jun. 2017.
[37] D. Kim and J. Lee, "Integrated topology management in flying ad hoc networks: Topology construction and adjustment," *IEEE Access*, vol. 6, pp. 61196–61211, 2018.
[38] G. Wu, W. Pedrycz, H. Li, M. Ma, and J. Liu, "Coordinated planning of heterogeneous Earth observation resources," *IEEE Trans. Syst., Man, Cybern. Syst.*, vol. 46, no. 1, pp. 109–125, Jan. 2016.
[39] I.-M. Chao, B. L. Golden, and E. A. Wasil, "The team orienteering problem," *Eur. J. Oper. Res.*, vol. 88, no. 3, pp. 464–474, Feb. 1996.
[40] I.-M. Chao, B. L. Golden, and E. A. Wasil, "A fast and effective heuristic for the orienteering problem," *Eur. J. Oper. Res.*, vol. 88, no. 3, pp. 475–489, Feb. 1996.
[41] A. Banks, J. Vincent, and C. Anyakoha, "A review of particle swarm optimization. Part II: Hybridisation, combinatorial, multicriteria and constrained optimization, and indicative applications," *Natural Comput.*, vol. 7, no. 1, pp. 109–124, Mar. 2008.
[42] H.-L. Shieh, C.-C. Kuo, and C.-M. Chiang, "Modified particle swarm optimization algorithm with simulated annealing behavior and its numerical verification," *Appl. Math. Comput.*, vol. 218, no. 8, pp. 4365–4383, Dec. 2011.
[43] M. Locatelli, "Convergence properties of simulated annealing for continuous global optimization," *J. Appl. Probab.*, vol. 33, no. 4, pp. 1127–1140, Dec. 1996.
[44] D. Mitra, F. Romeo, and A. Sangiovanni-Vincentelli, "Convergence and finite-time behavior of simulated annealing," *Adv. Appl. Probab.*, vol. 18, no. 3, pp. 747–771, Sep. 1986.
[45] C. Archetti, A. Hertz, and M. G. Speranza, "Metaheuristics for the team orienteering problem," *J. Heuristics*, vol. 13, no. 1, pp. 49–76, Feb. 2007.
[46] L. Ke, C. Archetti, and Z. Feng, "Ants can solve the team orienteering problem," *Comput. Ind. Eng.*, vol. 54, no. 3, pp. 648–665, Apr. 2008.
[47] D.-C. Dang, R. N. Guibadj, and A. Moukrim, "An effective PSO-inspired algorithm for the team orienteering problem," *Eur. J. Oper. Res.*, vol. 229, no. 2, pp. 332–344, Sep. 2013.
[48] S. Lin, "Solving the team orienteering problem using effective multi-start simulated annealing," *Appl. Soft Comput.*, vol. 13, no. 2, pp. 1064–1073, Feb. 2013.
[49] H. Bouly, D.-C. Dang, and A. Moukrim, "A memetic algorithm for the team orienteering problem," *4OR*, vol. 8, no. 1, pp. 49–70, Mar. 2010.
[50] R. Stone, "Wenchuan earthquake. A deeply scarred land," *Science*, vol. 324, pp. 713–714, May 2009.

MONING ZHU received the B.S. degree from the Beijing Institute of Graphic and Communication, in 2002, and the M.S. degree from the Hefei University of Technology, in 2012, where he is currently pursuing the Ph.D. degree with the School of Management. His research interests include UAV task assignment and routing planning.

XIAOXIA DU received the M.S. degree from the Nanjing University of Science and Technology, in 2005, and the Ph.D. degree from the Beijing University of Technology, in 2016. She is currently with National Earthquake Response Support Service, Ministry of Emergency Management, China. Her research interests include emergency response and rescue technology of earthquake disaster.

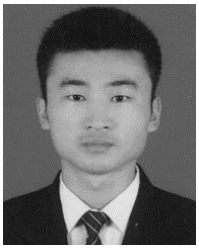

XUEHUA ZHANG received the B.S. degree from the Shandong University of Technology, in 2014, and the M.S. degree from the Institute of Earthquake Forecasting, CEA, in 2017. He is currently a Researcher with the National Earthquake Response Support Service. His research interests include the application of UAV remote sensing in earthquake emergency and disaster loss assessment.

HE LUO received the B.S. and Ph.D. degrees from the Hefei University of Technology, in 2004 and 2009, respectively, where he is currently a Professor. His research interests include intelligent decision making, multi-agent systems, and the applications of unmanned aerial vehicle.

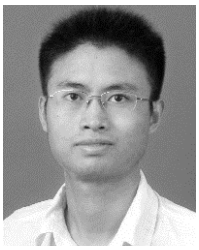

GUOQIANG WANG received the B.S. and M.S. degrees from the University of Science and Technology of China, in 2004 and 2007, respectively, and the Ph.D. degree from the Hefei University of Technology, in 2016, where he is currently a Lecturer. His research interests include management and intelligent decision making of unmanned aerial vehicle formation.